ESD-TR-79-284

Technical Note

1979-82

See 1473 in back.

A Simple Graphical Model for Analyzing Radar Homing Interceptor Engagements

S. D. Weiner

17 December 1979

Prepared for the Department of the Army
under Electronic Systems Division Contract F19628-80-C-0002 by

Lincoln Laboratory
MASSACHUSETTS INSTITUTE OF TECHNOLOGY
LEXINGTON, MASSACHUSETTS

The work reported in this document was performed at Lincoln Laboratory, a center for research operated by Massachusetts Institute of Technology. This program is sponsored by the Ballistic Missile Defense Program Office, Department of the Army; it is supported by the Ballistic Missile Defense Advanced Technology Center under Air Force Contract F19628-80-C-0002.

The views and conclusions contained in this document are those of the contractor and should not be interpreted as necessarily representing the official policies, either expressed or implied, of the United States Government.

This technical report has been reviewed and is approved for publication.

FOR THE COMMANDER

Raymond L. Loiselle

Raymond L. Loiselle, Lt. Col., USAF
Chief, ESD Lincoln Laboratory Project Office

MASSACHUSETTS INSTITUTE OF TECHNOLOGY

LINCOLN LABORATORY

A SIMPLE GRAPHICAL MODEL FOR ANALYZING RADAR HOMING INTERCEPTOR ENGAGEMENTS

S. D. WEINER

Group 32

TECHNICAL NOTE 1979-22

17 DECEMBER 1979

LEXINGTON MASSACHUSETTS

ABSTRACT

In this note, a simplified model of radar homing interceptor engagements is described. This model permits analysis of the interaction among sensor parameters such as angular accuracy and acquisition range, interceptor parameters such as maneuver limits and response time and system parameters such as closing velocity and handover accuracy. Simple expressions are obtained for the sensor prediction accuracy using various types of range-dependent measurement errors. These include glint, instrumentation error and thermal error for both active and semi-active sensors. A simple graphical technique is used to determine the feasibility of a homing engagement and to estimate the resulting miss-distance. A set of nomograms is included to permit full variation of the system and component parameters

CONTENTS

I. INTRODUCTION

There is considerable interest in missiles using radar homing sensors for both tactical and strategic applications. In this note, we will present a simplified model of the homing engagement to illustrate the interaction among the various parameters characterizing system performance. The primary motivation for this study came from consideration of non-nuclear interception of stategic reentry vehicles but much of the analysis should be applicable to problems of intercepting aircraft or of attacking ground targets.

The model makes use of graphical comparison of the accuracy of the predicted intercept point and the interceptor divert capability to determine whether an intercept is feasible and, if it is, to estimate the resulting miss-distance.

The sensor prediction accuracy depends on the sensor measurement accuracy and its variation with range to the target, the acquisition range at which tracking starts, the instantaneous range at which tracking stops and prediction starts and the data rate over the tracking interval. We will obtain graphs of prediction accuracy as a function of the range to the target. The prediction accuracy improves (the error decreases) as the range to the target decreases.

The capability of the interceptor to correct for any predicted error is a function of its maneuver limits, its response time and the time remaining until intercept. At sufficiently

close ranges, the interceptor is no longer capabable of fully correcting the prediction error and this residual error is a rough approximation to the miss-distance.

Near acquistion, the homing sensor prediction error is larger than the interceptor divert capability and, unless the handover accuracy is sufficiently good, it will not be possible to close out the initial error.

In the next section, we describe the sensor error models assumed and the resulting prediction errors. In section III, we present the interceptor divert model used. Section IV contains several applications of this model to illustrate the dependence of system performance on component performance and the engagement scenario. We give a brief discussion of the results in section V. There are several appendices containing detailed calculations and instructions for constructing nomograms to permit graphical analysis for a variety of cases.

In reading this note, the reader should be aware that a number of simplifing assumptions have been made. There are a number of measurement, computational and guidance functions which have been assumed implicitly in this model; some of them will be discussed in later sections.

II. SENSOR MODEL

In this section we calculate the prediction error for a homing sensor which tracks a target from the acquisition range, R_A, to a given range, R, and predicts ahead to intercept (range = 0). We work in a coordinate system on the interceptor so that the target velocity is the closing velocity, V_c. The sensor measures the position of the target on each pulse to an accuracy σ_R which, in general, is a function of range. For simplicity we will use a linear approximation to the target trajectory. In principle, we could linearize about a nominal trajectory to obtain equivalent performance but in practice uncertainties in target drag or interceptor acceleration will limit the accuracy achievable. Some of these problems are discussed in Ref. 1. Our purpose here is to illustrate the effect of sensor measurement accuracy on homing performance and a linear model is the simplest way to show this.

Prediction Accuracy

The problem we are addressing is the following: The radar makes a sequence of measurements of target position, Z_i (i=1,...N) at ranges R_i with accuracy σ_i and fits a straight line trajectory through these points, $y = a_0 + a_1 R$. The constants a_0 and a_1 are chosen to minimize the sum of the squares of the weighted residuals

$$J = \sum_{i=1}^{N} [Z_i - (a_0 + a_1 R_i)]^2 / \sigma_i^2$$

The target position Z_i can be any component of the position (i.e., range or cross-range). In general, the angular errors will have greater contribution to the miss-distance and we will generally deal with measurements in the cross-range direction. The estimated position of the target at the intercept point is given by $y(R=0) = a_0$. In Appendix 1, we show that the estimate of a_0 is

$$a_0 = \frac{\sum \frac{Z_i}{\sigma_i^2} \sum \frac{R_i^2}{\sigma_i^2} - \sum \frac{R_i Z_i}{\sigma_i^2} \sum \frac{R_i}{\sigma_i^2}}{\sum \frac{1}{\sigma_i^2} \sum \frac{R_i^2}{\sigma_i^2} - \left(\sum \frac{R_i}{\sigma_i^2}\right)^2} \qquad (1)$$

and the variance of this estimate is

$$\mathrm{Var}(a_0) = \frac{\sum \frac{R_i^2}{\sigma_i^2}}{\sum \frac{1}{\sigma_i^2} \sum \frac{R_i^2}{\sigma_i^2} - \left(\sum \frac{R_i}{\sigma_i^2}\right)^2} \qquad (2)$$

where the summations are over all measurements. The prediction error is the square root of $\mathrm{Var}(a_0)$. More general versions of Eqs. (1) and (2) are contained in Ref. 1.

In the rest of this section, we will consider the prediction error resulting from various types of measurement error $\sigma_i=\sigma(R_i)$. To obtain relatively simple expressions for $\mathrm{Var}(a_0)$, we will replace the summations in Eq. (2) by integrals.* If measurements are taken at a rate given by the pulse repetition frequency (prf), then we can replace

$$\sum_{i=1}^{N}$$

by

$$\frac{prf}{V_c}\int_{R}^{R_A} dR$$

where V_c is the closing velocity (the relative velocity between target and interceptor). In this case, Eq. (2) becomes

$$\mathrm{Var}(a_0) = \frac{V_c}{prf}\,\frac{\int \frac{R^2}{\sigma_R^2}\,dR}{\int \frac{dR}{\sigma_R^2}\int \frac{R^2}{\sigma_R^2}\,dR - \left(\int \frac{R}{\sigma_R^2}\,dR\right)^2} \qquad (3)$$

where all integrals go from R_A to R.

We now proceed to evaluate Eq. (3) for various cases of $\sigma_R(R)$.

*I am indebted to Dr. C. B. Chang for suggesting this procedure.

Error Models

Often the angular error of a radar is expressed as the sum of three terms

$$\text{Error} = \text{Glint Error} + \text{Instrumentation Error} + \text{Thermal Error} \quad (4)$$

The glint error is due to the fact that the target is not a point scatterer and interference among different scattering centers on the target will cause the radar estimate of the target position to vary. The magnitude of this error is comparable with the target dimensions and is independent of range.

The thermal error is determined by the signal-to-noise ratio (S/N) and is typically

$$\frac{\text{Beamwidth}}{2\sqrt{S/N}}$$

in angular units. The resulting position error is obtained by multiplying the angular error by the range. For an active sensor, S/N varies as R^{-4} so the position error varies as R^3. For a semi-active sensor, S/N varies as R^{-2} (assuming the illuminator is relatively far from the target and interceptor) and the position error varies as R^2.

The instrumentation error is what is left over. It is the error on a point target at infinite signal-to-noise ratio. In-

strumentation error can result from antenna errors, interceptor vibration, plasma effects, etc. In angular units, this error is independent of range so the position error varies as R.

The four types of errors to be considered are listed below.

Case 0	$\sigma_R = \sigma$	Glint
Case 1	$\sigma_R = \sigma_\theta R$	Instrumentation
Case 2	$\sigma_R = \sigma_A \ (R^2/R_A)$	Thermal (Semi-active)
Case 3	$\sigma_R = \sigma_A \ (R^3/R_A^2)$	Thermal (Active)

In these cases, σ has units of meters, σ_θ and σ_A have units of radians; σ_A is the angular error at acquisition ($R=R_A$). Substituting the above expressions for σ_R into Eq. (3), we obtain the following expressions for $\mathrm{Var}(a_o)$ which is the square of the prediction error.

$$\text{Case 0} \qquad \mathrm{Var}(a_o) = \frac{4\ V_c\ \sigma^2}{prf \cdot R_A} \ \frac{y^3+y^2+y}{(y-1)^3} \tag{5a}$$

$$\text{Case 1} \qquad \mathrm{Var}(a_o) = \frac{V_c\ \sigma_\theta^{\,2}\ R}{prf} \ \frac{y-1}{y+(1/y)-2-(\ln y)^2} \tag{5b}$$

$$\text{Case 2} \qquad \mathrm{Var}(a_o) = \frac{12\, V_c\, \sigma_A^2\, R^3}{prf \cdot R_A^2} \frac{y^3}{(y-1)^3} \tag{5c}$$

$$\text{Case 3} \qquad \mathrm{Var}(a_o) = \frac{80\, V_c\, \sigma_A^2\, R^5}{prf \cdot R_A^4} \frac{y^5(y^2+y+1)}{(y-1)\left[(y^3+y^2+y+1)^2-16y^3\right]} \tag{5d}$$

where $y \equiv R_A/R$. The derivation of these equations is given in Appendix 2.

Equations (5a) - (5d) have been written to explicitly show the dependence of $\mathrm{Var}(a_o)$ on R as $R \to 0$. ($y \to \infty$). In this limit, the factors involving y go to unity indicating that the prediction error is independent of R for glint, varies as $R^{\frac{1}{2}}$ for instrumentation error and as either $R^{3/2}$ or $R^{5/2}$ for thermal error.

Eqs. (5b) - (5d) can be rewritten in terms of σ_R as

$$\text{Case 1} \qquad \mathrm{Var}(a_o) = \frac{V_c\, \sigma_R^2}{prf \cdot R} f(y)$$

$$\text{Case 2} \qquad \mathrm{Var}(a_o) = \frac{12\, V_c\, \sigma_R^2}{prf \cdot R} g(y)$$

$$\text{Case 3} \qquad \mathrm{Var}(a_o) = \frac{80\, V_c\, \sigma_R^2}{prf \cdot R} h(y)$$

with f,g and h being the expressions in Eqs. (5b) - (5d).

The other limiting case, $R \to R_A$ ($y \to 1$) is less transparent. In Appendix 2 we show that for all cases

$$\mathrm{Var}(a_o) \to \frac{12\, V_c\, R^2\, \sigma_R^2}{\mathrm{prf}\ (R_A - R)^3} \quad \text{as } R \to R_A \tag{6}$$

In this limit, the prediction error varies as $(R_A-R)^{-3/2}$. This dependence can be understood physically as follows. The tracking baseline which is used for extrapolation is proportional to (R_A-R) giving a factor of $(R_A-R)^{-1}$ in the prediction error. The number of pulses in the tracking interval is also proportional to (R_A-R) and since the effect of smoothing these pulses decreases the error by the square root of the number of pulses, this supplies the additional factor of $(R_A-R)^{-\frac{1}{2}}$.

Figures 1-4 show the prediction error (the square root of the variance) as a function of R for several values of R_A. These figures are obtained from Eqs. (5a) - (5d) and can be scaled to different values of V_c, prf, and the various σ's using these equations. The nomogram kit contained in Appendix 3 can be used to perform calculations for other sets of parameter values.

We can approximate the prediction error resulting from all sources by taking the variance of Eq. (4). If the error sources are independent, we can take the root-sum-square of the error due to the individual terms. This is done graphically in Fig. 5 for a specific case. It is seen that thermal error is most severe at

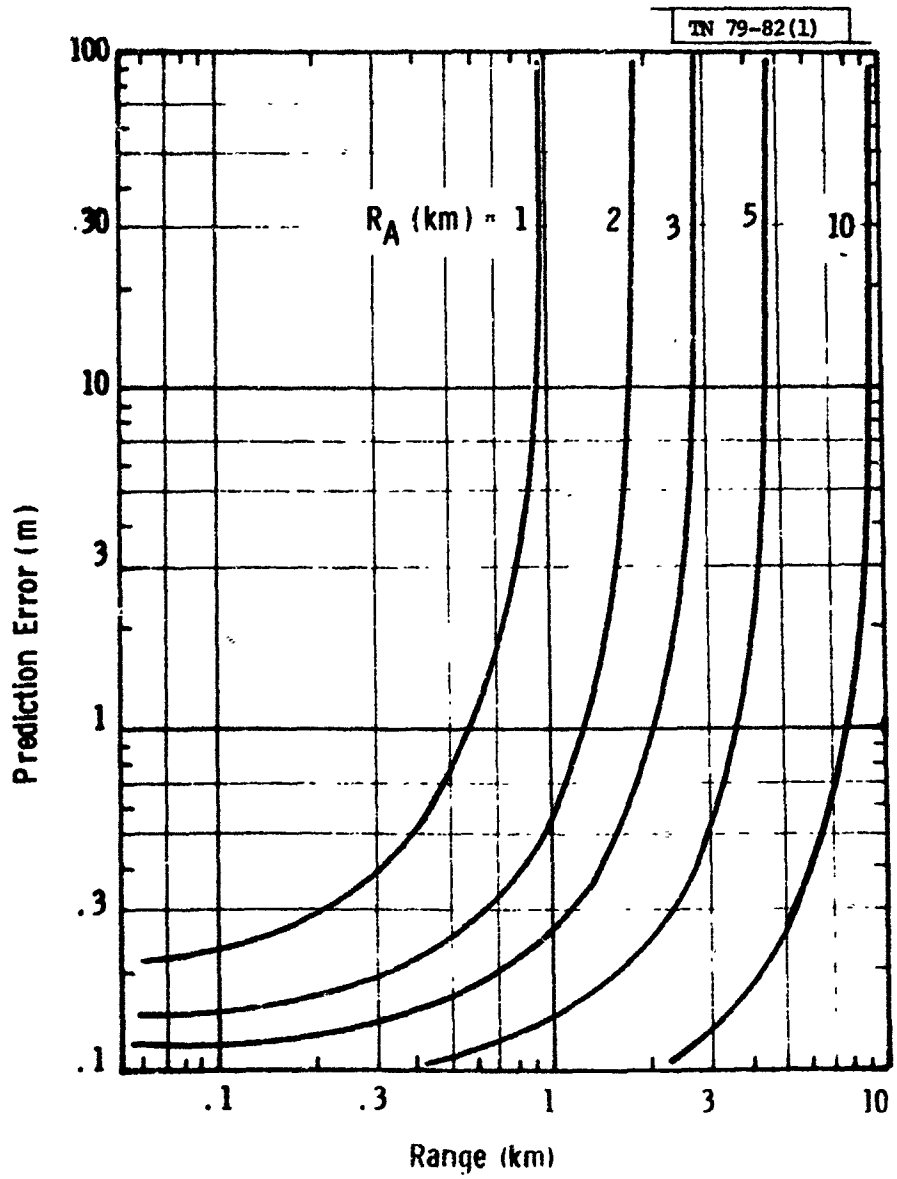

Glint σ = 1 m
prf = 100
V_c = 1 km/sec

Fig. 1. Prediction error - glint.

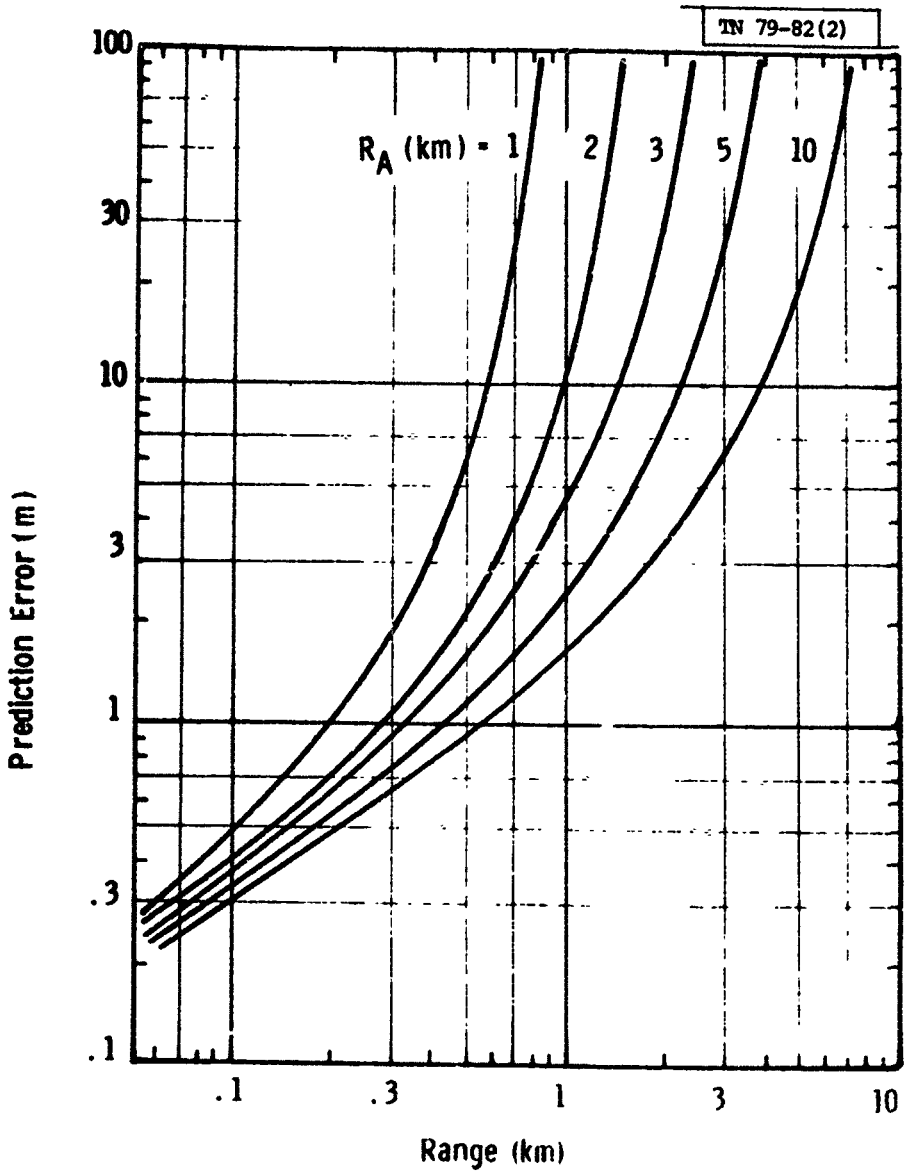

Fig. 2. Prediction error - instrumentation.

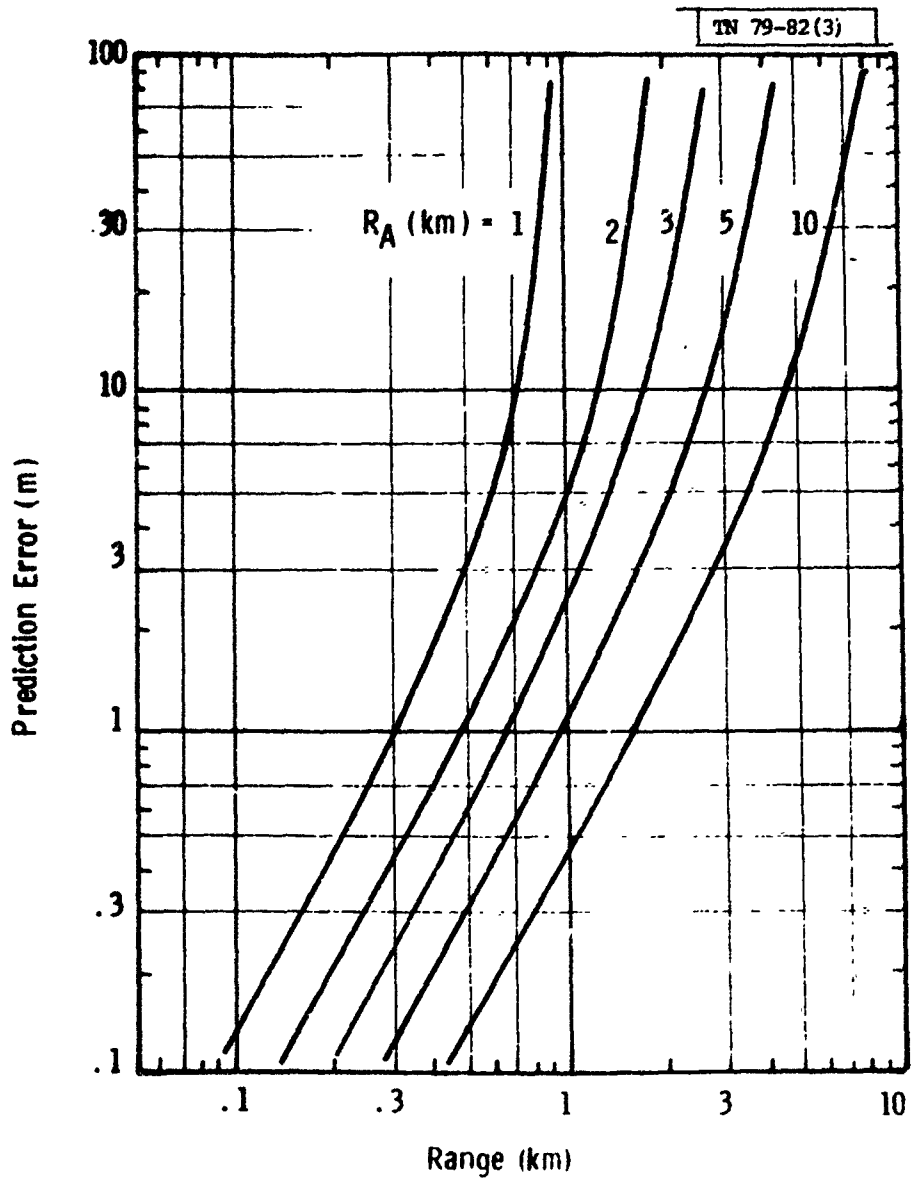

Thermal	σ_A	= 10 mr
(Semi -	prf	= 100
Active)	V_c	= 1 km/sec

Fig. 3. Prediction error - thermal (semi-active).

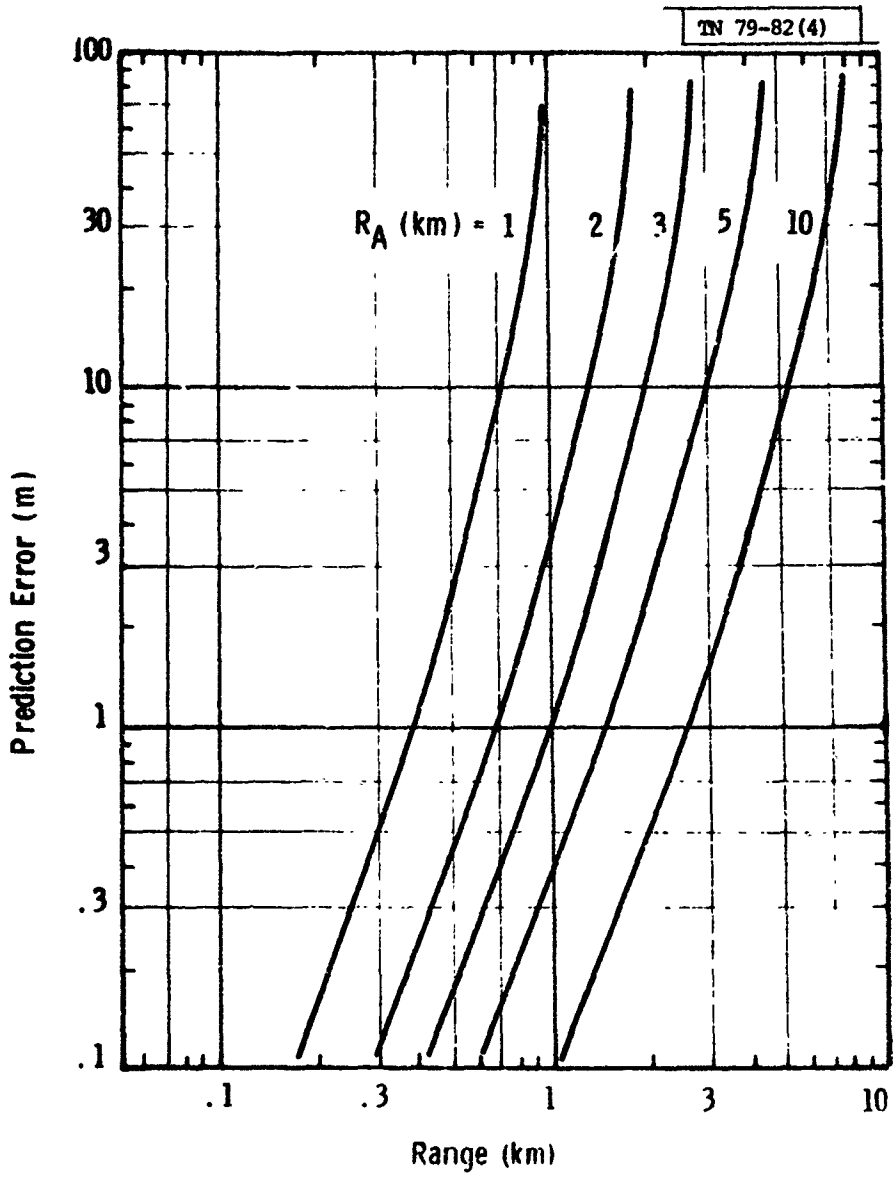

Fig. 4. Prediction error - thermal (active).

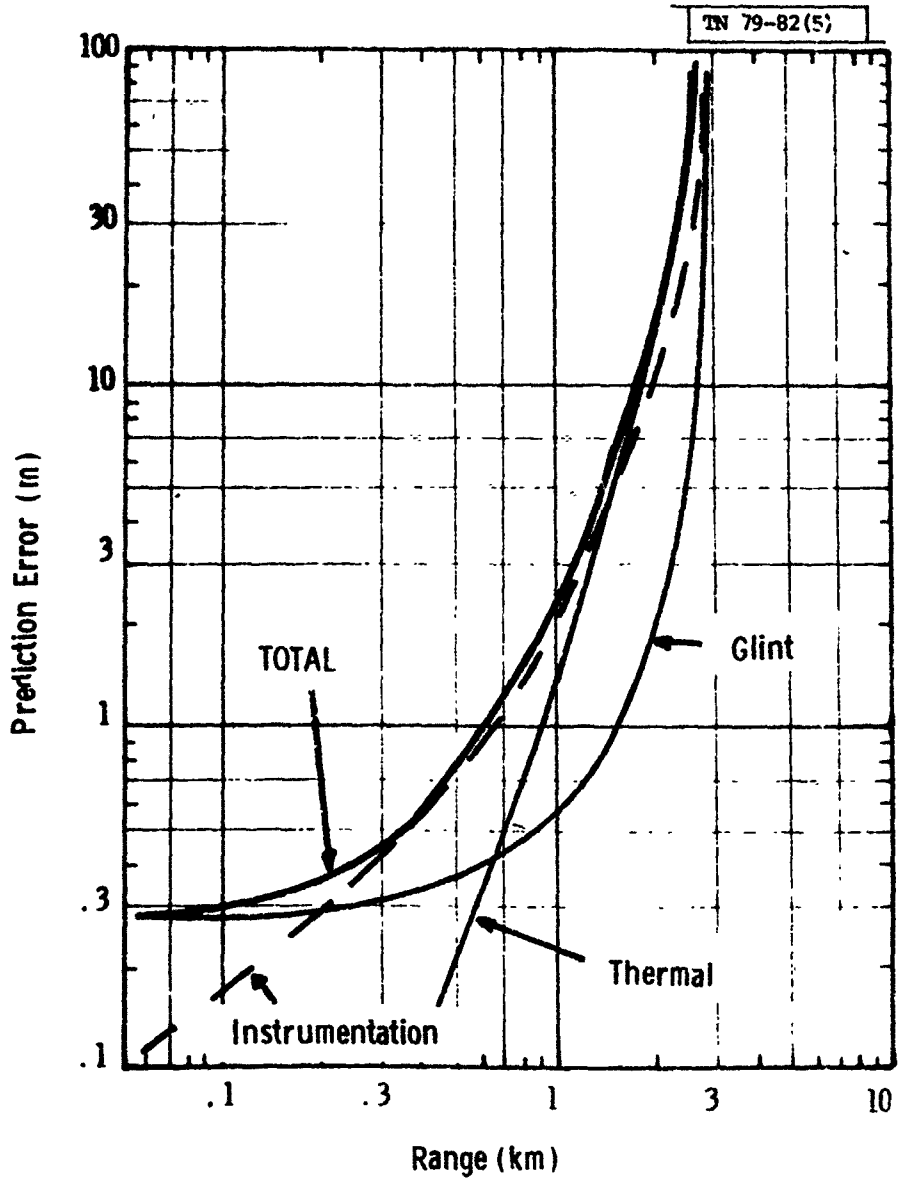

Fig. 5. Combined prediction error.

long ranges while glint is worst at short ranges.

III. INTERCEPTOR MODEL

The two major characteristics of the interceptor which we wish to model are its maneuver acceleration limit and its response time. (One other interceptor parameter, the command bias, and its influence on miss distance was discussed in Ref. 1.) Here we will show that the missile response time, τ, has a major influence on miss-distance while the acceleration limit has a major influence on the handover accuracy required.

We model the response of the interceptor to a commanded acceleration at time zero as consisting of zero acceleration until time τ followed by constant acceleration (bounded by the maneuver limit, a). Thus the divert capability of the interceptor is

$$\tfrac{1}{2}\, a\, (t-\tau)^2$$

The maximum error which can be corrected during an engagement is limited by the time remaining until intercept. This time is R/V_c so that

$$\text{Divert} = \frac{a}{2}\left(\frac{R}{V_c} - \tau\right)^2 \qquad (7)$$

Figure 6 shows the divert capability as a function of R for

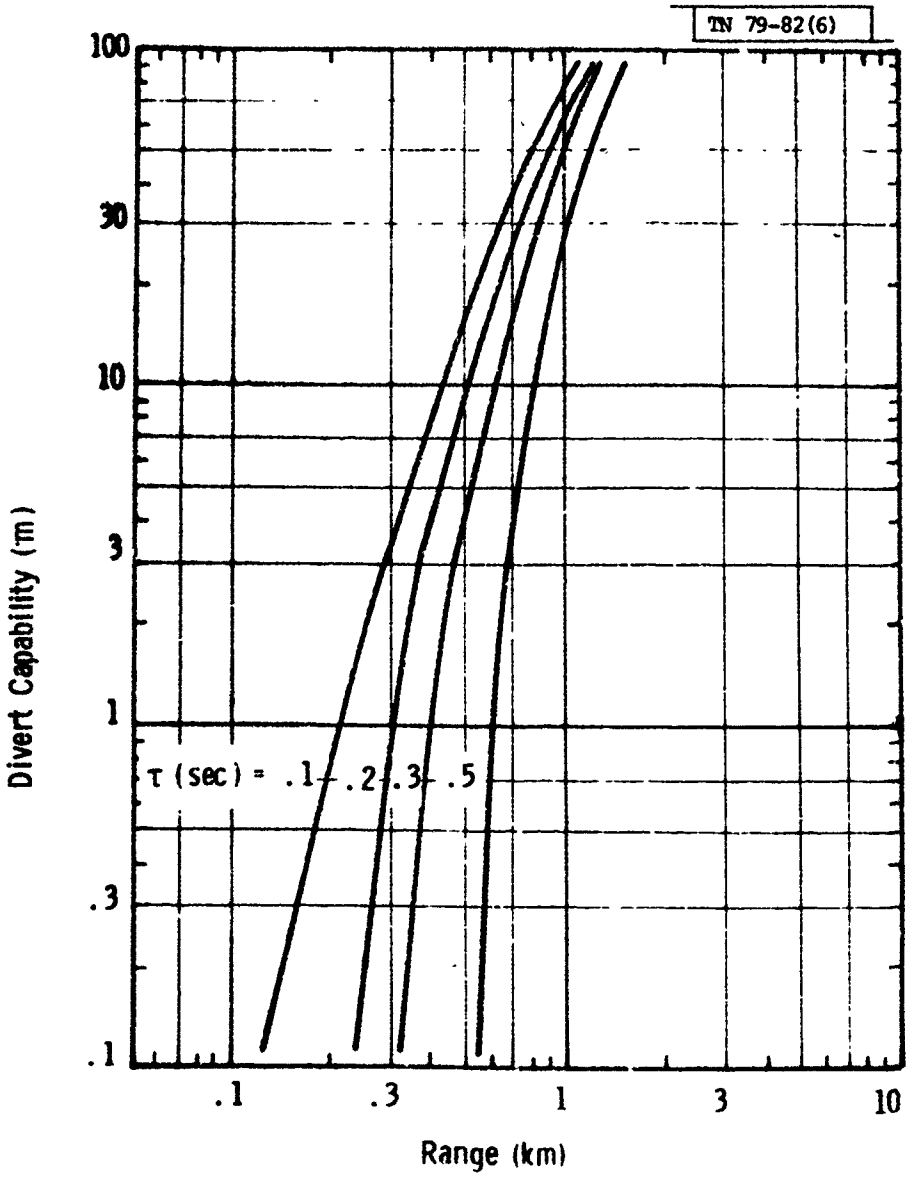

Fig. 6. Interceptor divert.

several values of τ. These cases can be scaled to different values of V_c and a using Eq. (7). The nomogram kit contained in Appendix 3 can be used to examine other cases graphically.

IV. ENGAGEMENT MODEL AND APPLICATIONS

In this section, we will see how the sensor and interceptor models described above can be combined to give an engagement model. This will be illustrated using the sensor prediction error curve from Fig. 5 combined with one of the interceptor divert curves from Fig. 6. We further assume a handover accuracy of 30m. The parameters describing the engagement are listed in Table 1.

TABLE 1

ENGAGEMENT PARAMETERS

Closing Velocity		5 km/sec.
Handover Accuracy		30 m
Sensor Acquisition Range		3 km
	prf	100
	Glint Error	1 m
	Instrumentation Error	2 mr
	Thermal Error (Active)	5 mr
Interceptor:	Response Time	.1 sec
	Acceleration Limit	100 g

We can follow the engagement as the range decreases in Fig. 7. At long range (prior to sensor acquisiton) the prediction

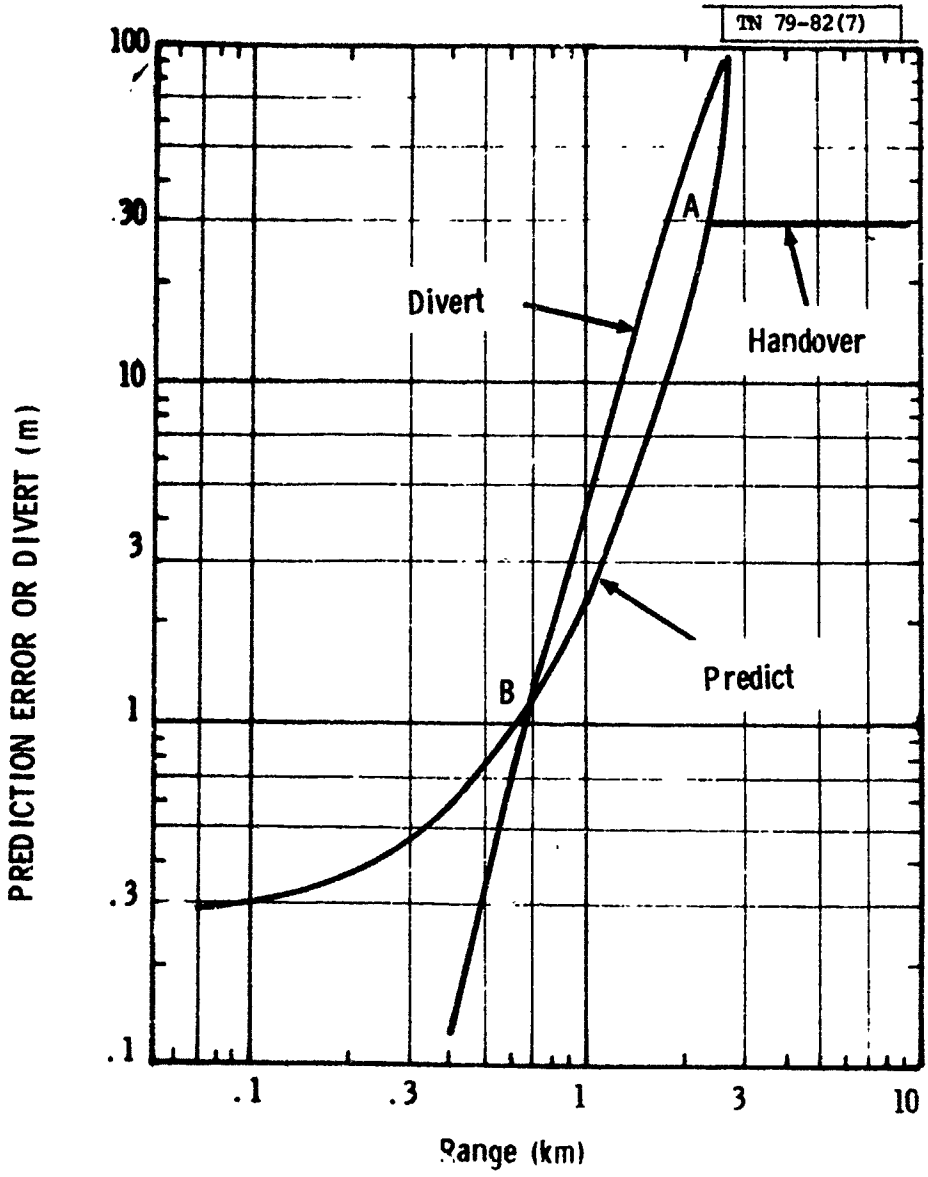

Fig. 7. Sample engagement.

error is limited by the handover accuracy. The interceptor divert capability can take out this error. At point A, the data from the homing sensor is sufficiently accurate to reduce the prediciton error. As R decreases, both the sensor prediction error and the interceptor divert capability decrease. At point B, the divert is just adequate to take out the prediction error. To the left of B, the prediction error continues to decrease but the divert capability is insufficient. The prediction error at point B is of the order of 1.3 m and we will use this as an estimate of the miss-distance.

It must be kept in mind that we are dealing with statistical quantities rather than deterministic ones so that the crossing points of the various curves represent expected values (at best). For any particular engagement, it is possible that the actual prediction error to the left of point B could be less than the divert capability of the interceptor and so the actual miss distance would be less than 1.3 m. Conversely, it is possible that the actual prediction error to the right of point B could exceed the divert capability thus giving a larger miss-distance.

Before trying to relate system performance to component performance, it is useful to see which parameters influence which portions of the engagement. Fig. 8 compares two sensors (considering only the instrumentation error) showing that the prediciton error at short range is determined by the angular accuracy, σ_θ,

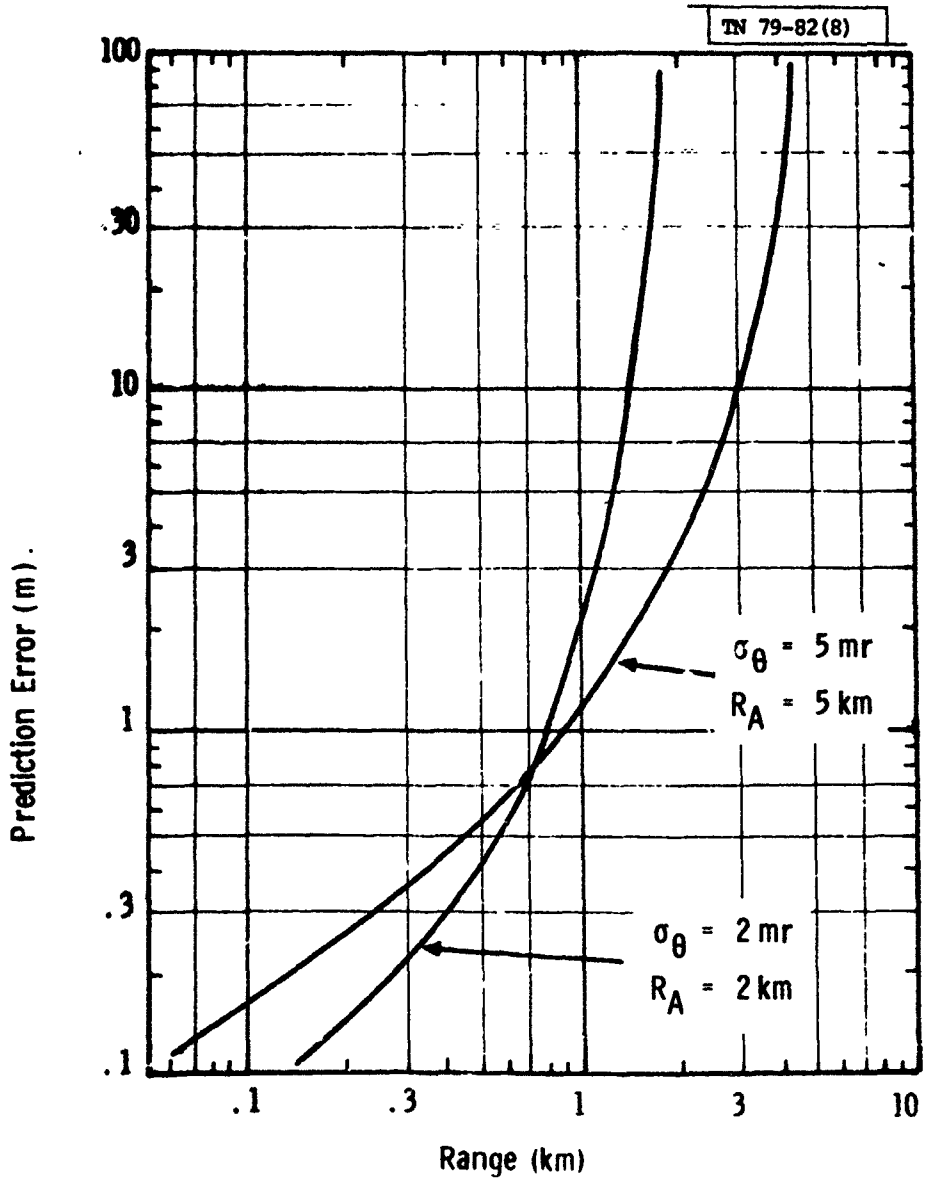

Fig. 8. Performance of different sensors.

and at long ranges is determined by the acquisition range, R_A. Similarly, Fig. 9 compares two interceptors showing that the divert capability at short range is determined primarily by the response time, τ, and at long range is determined by the acceleration limit, a.

We can now consider another sample engagement and indiciate how performance can be improved. Fig. 10 indicates a case where the handover accuracy is not sufficiently good for homing to be feasible. The shaded triangular region must be eliminated for successful intercept to be likely. This can be done in three ways (or in some combination of these). The first is to reduce the handover error to depress the top of the triangle. The second is to increase the sensor acquisition range to move the left side of the triangle to the right. The final approach is to increase the interceptor acceleration limit to raise the lower right side of the triangle.

We can also consider how the miss-distance represented by point B can be reduced. This intersection can be moved lower on the graph in two ways. The first is to reduce the sensor angular error and the second is to reduce the interceptor response time.*

Finally we wish to show how homing performance varies with the closing velocity, V_c. We consider a given sensor and inter-

*An alternate approach is to use an aimed warhead to kill the target without attempting to reduce the miss-distance.

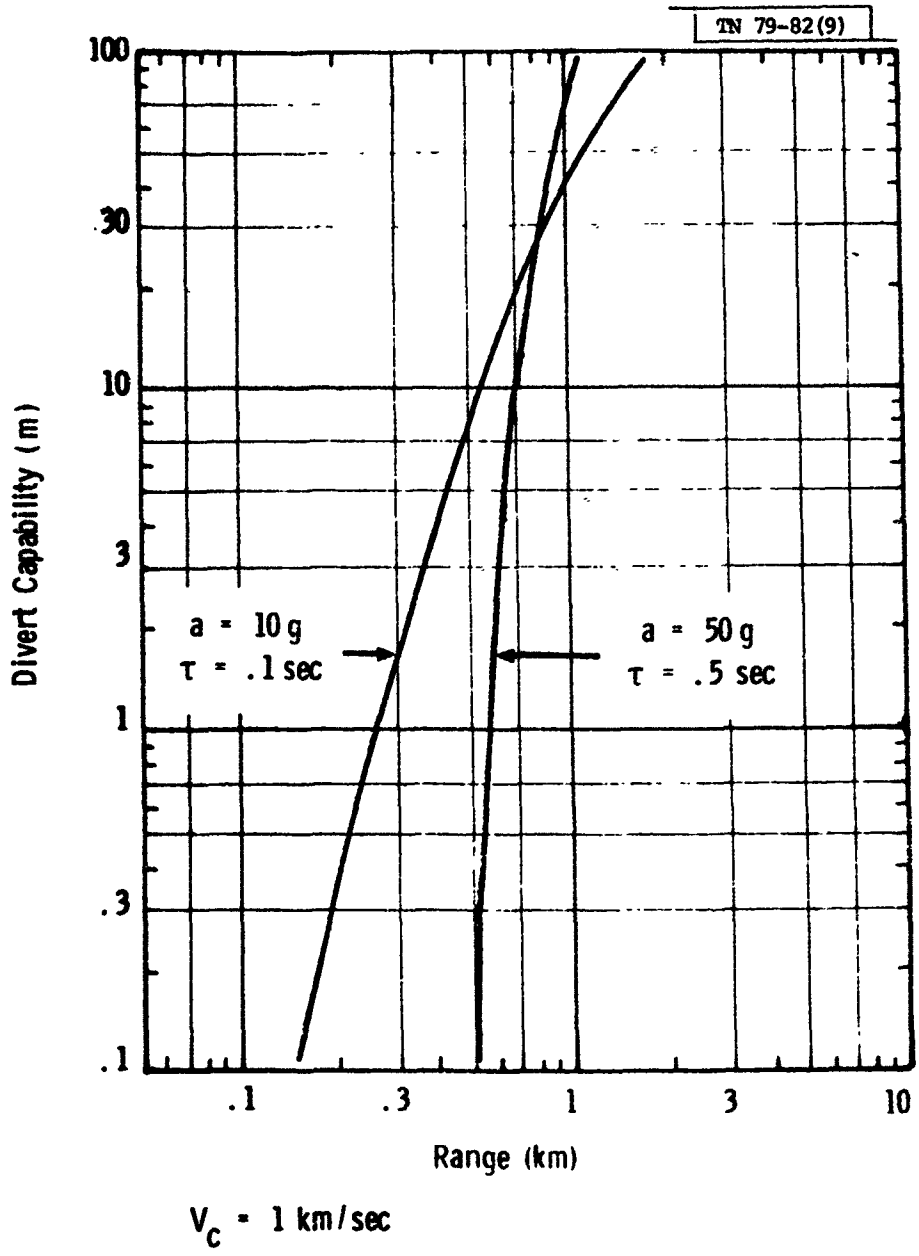

Fig 9. Performance of different interceptors.

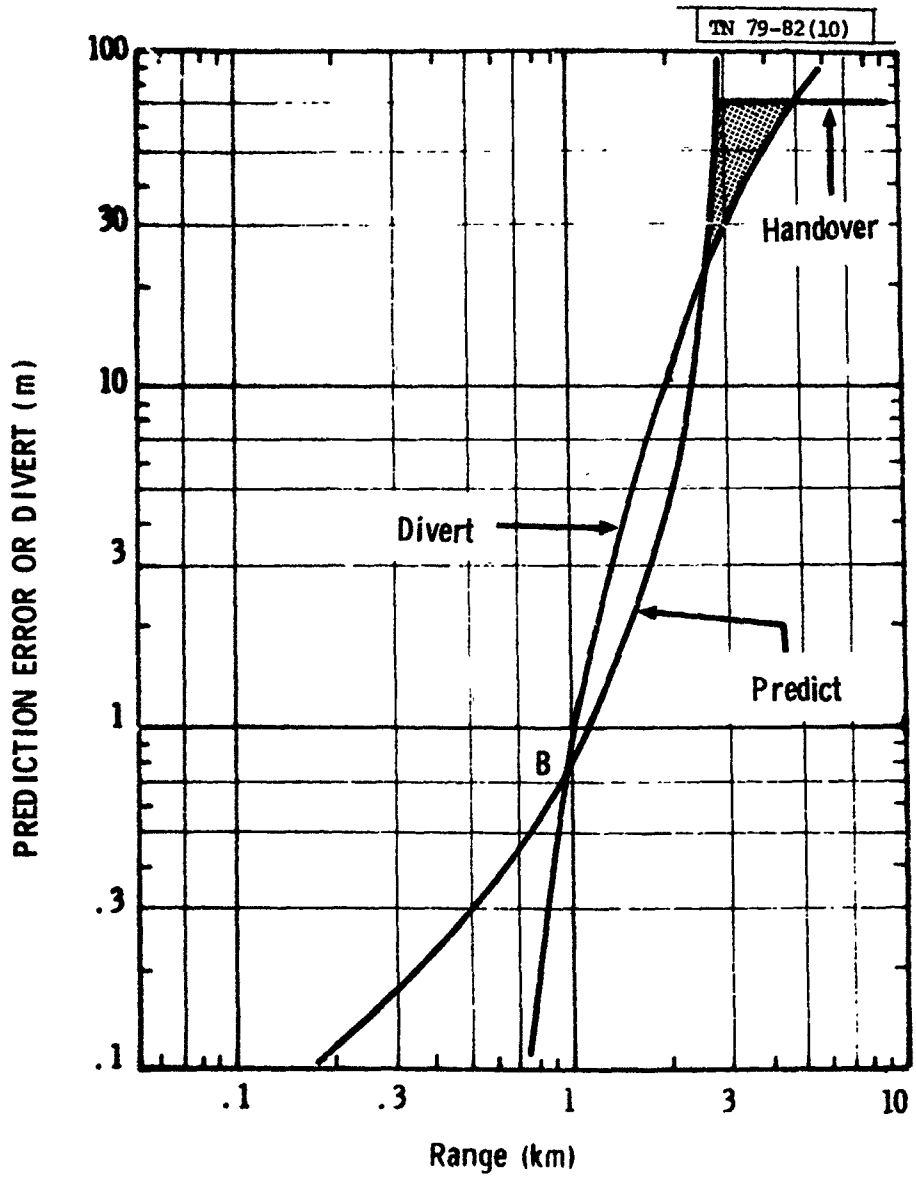

V_c = 3 km/sec R_A = 3 km

a = 10 g prf = 100

τ = .2 sec σ_θ = 1 mr

Fig. 10. Unsuccessful engagement.

ceptor characterized in Table 2.

TABLE 2

COMPONENT PARAMETERS

Sensor	Acquisition range	3 km
	Instrumentation error	5 mr
Interceptor	Response time	.3 sec.
	Acceleration limit	20 g

Figs. 11-13 show the prediction error and divert capability for three values of V_c. Where these curves have two intersections, the upper one determines the required handover accuracy while the lower one determines the miss distance. These quantities are shown as functions of V_c in Fig. 14. (These calculations are particularly simple using the nomograms described in Appendix 3.) For $V_c \gtrsim 3$ km/sec, the homing does not reduce the miss distance which would be achieved by the handover prediction alone.

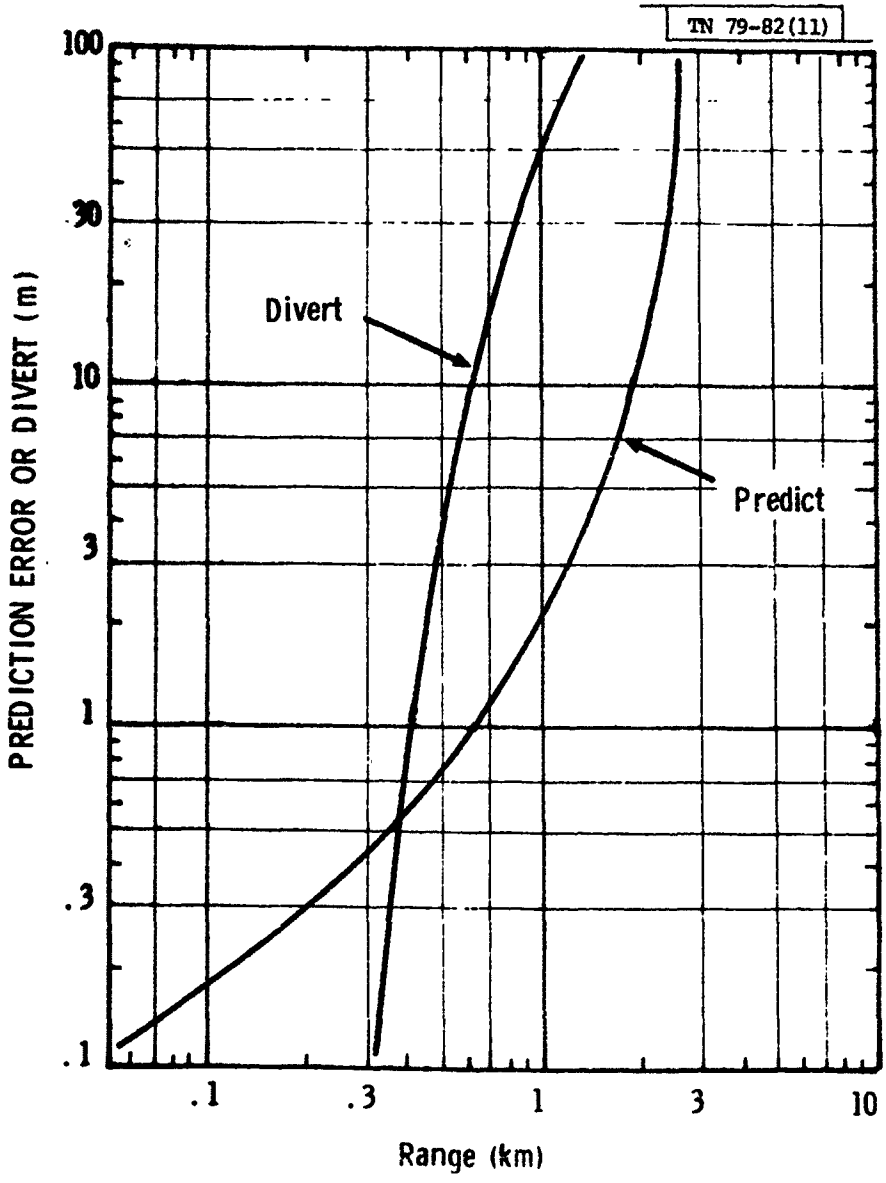

R_A = 3 km a = 20 g V_c = 1 km/sec

prf = 100 τ = .3 sec

σ_θ = 5 mr

Fig. 11. Engagement for V_c = 1 km/sec.

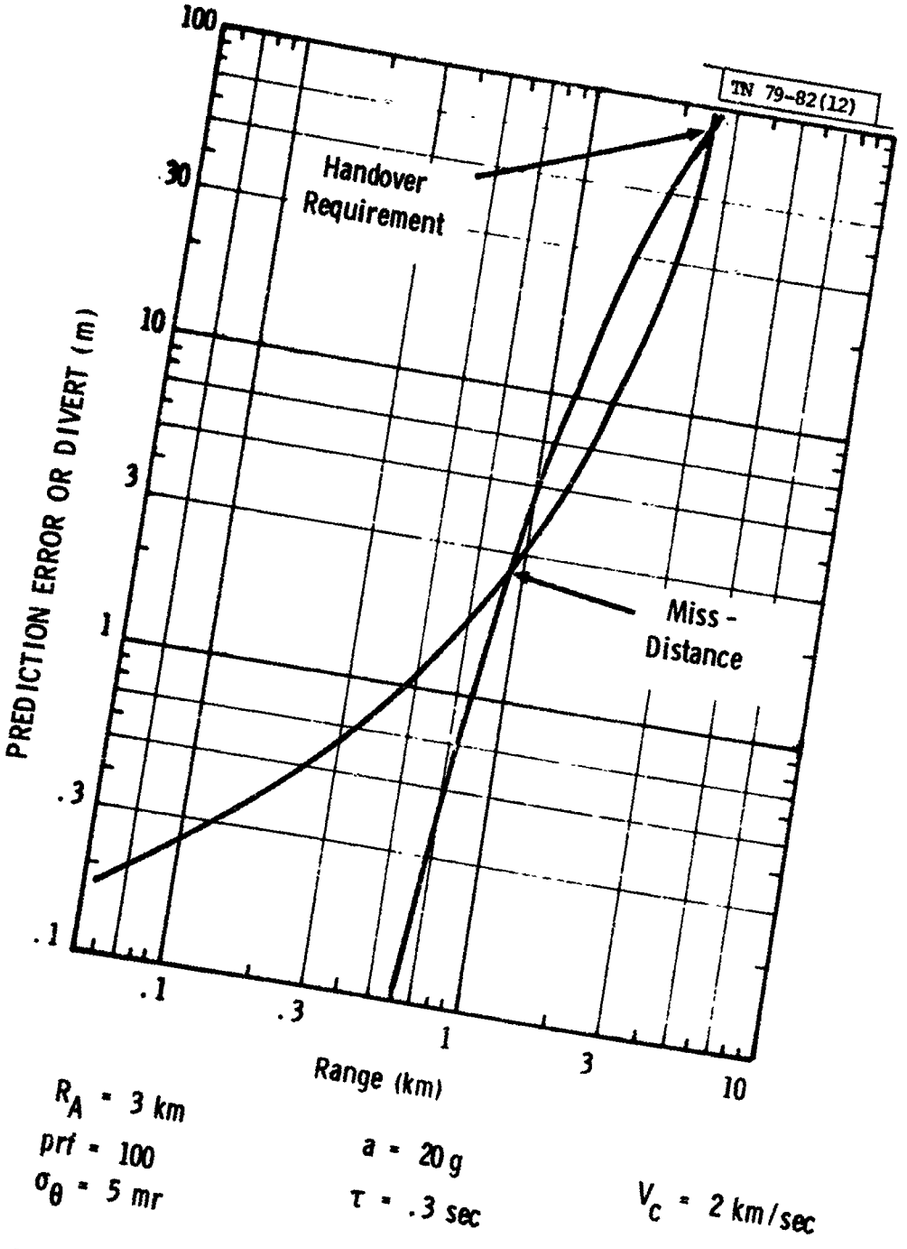

Fig. 12. Engagement for V_c = 2 km/sec.

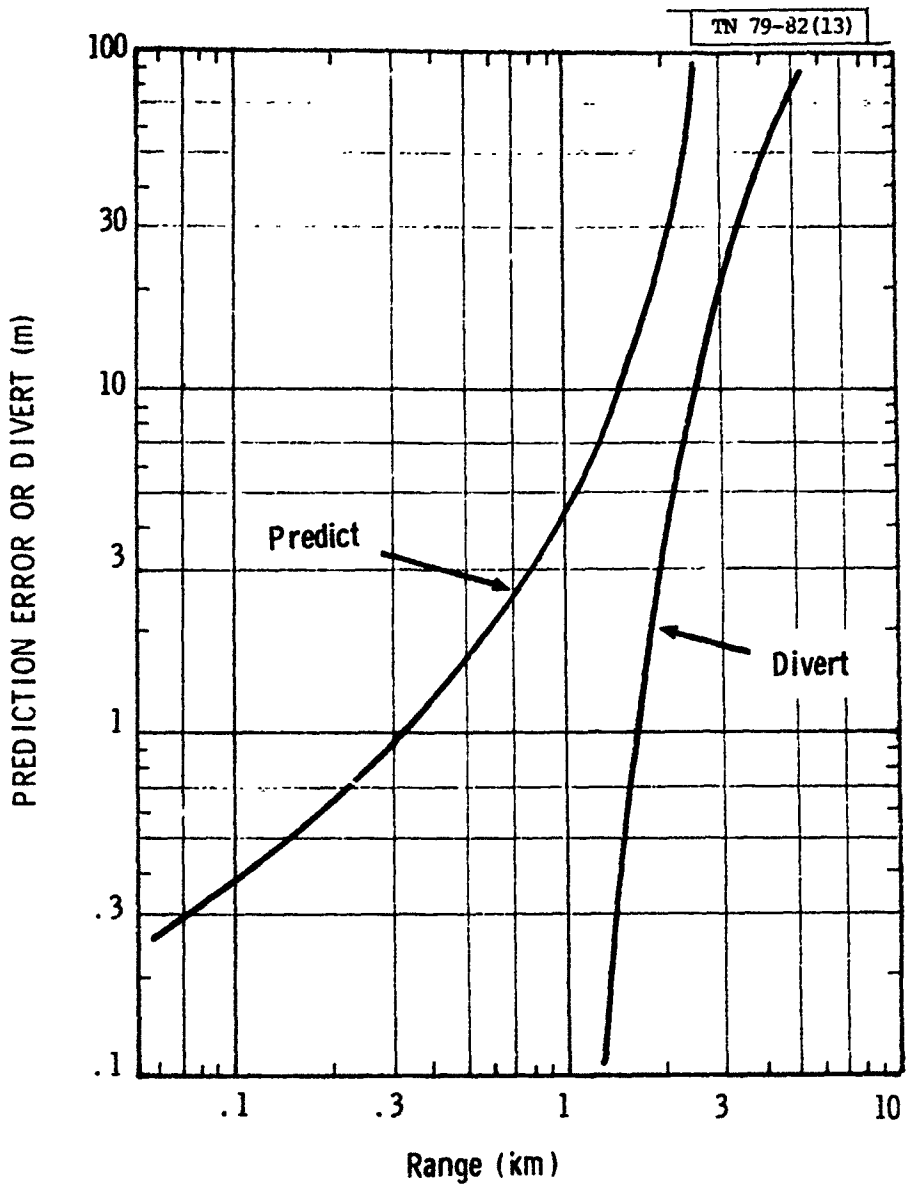

R_a = 3 km a = 20 g V_c = 4 km/sec
prf = 100 τ = .3 sec
σ_θ = 5 mr

Fig. 13. Engagement for V_c = 4 km/sec.

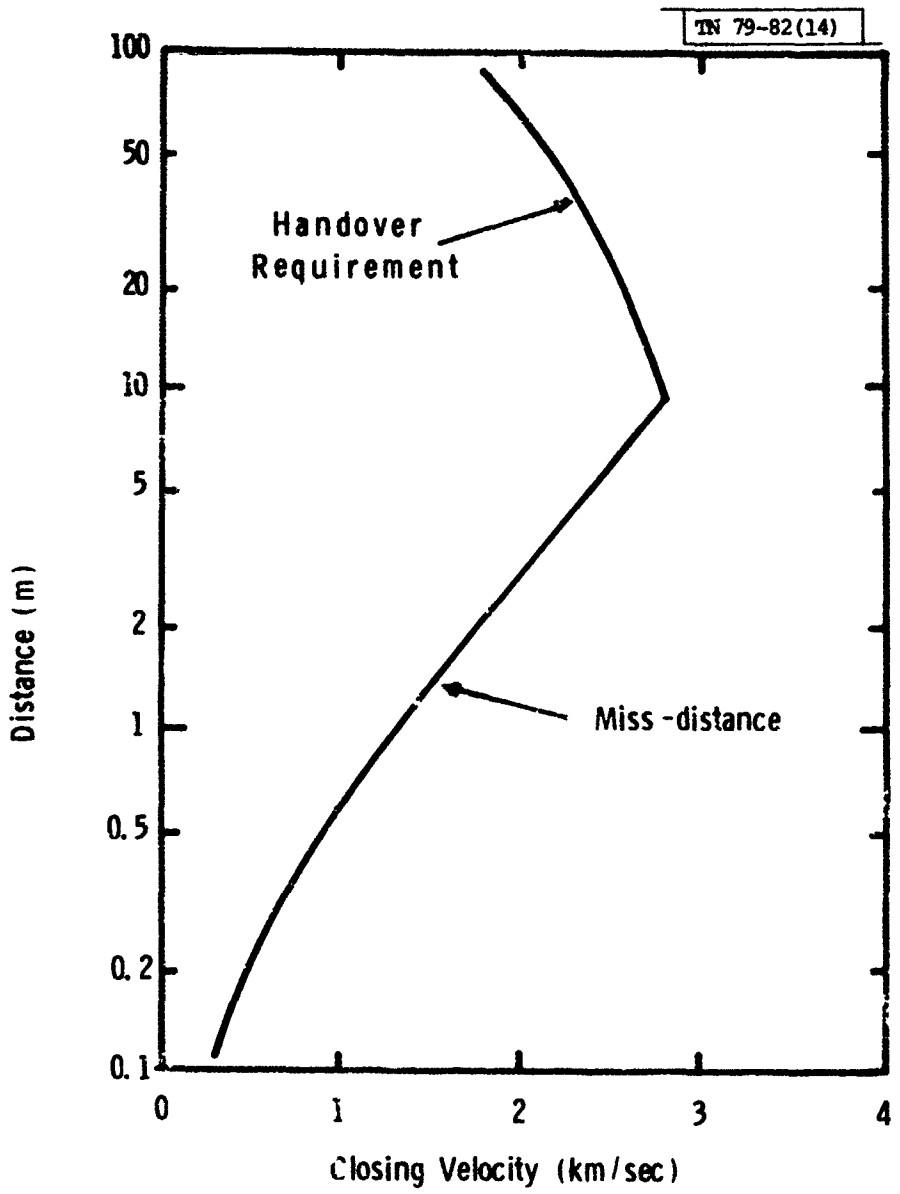

Fig. 14. Performance as function of closing velocity.

V. DISCUSSION

We have described a simple graphical model of a radar homing engagement which is useful for relating system performance (miss-distance) to component performance (sensor accuracy and range, interceptor response time and maneuver limit) and engagement scenario (closing velocity and handover accuracy). We conclude that the basic feasibility of homing is determined by the hand-over accuracy, the sensor acquisition range, the interceptor acceleration limit and the closing velocity. If homing is feasible, the resulting miss-distance is determined by the sensor accuracy, the interceptor response time and the closing velocity.

Directions for constructing a set of nomograms are included in Appendix 3. The reader is encouraged to make and play with these nomograms to get a feel for how the various parameters relate.

Finally, we repeat the caution that this model is highly simplified and should be used for qualitative rather the quantitative indication of system performance.

ACKNOWLEDGMENT

I wish to thank Drs. C. B. Chang, L. C. Kramer and D. Willner for many helpful discussions in connection with the work presented here.

REFERENCE

1. R. W. Miller and C. B. Chang, "Some Analytical Methods for Tracking, Prediction and Interception Performance Evaluations" (9 August 1977) (not generally available).

APPENDIX 1: Derivation of Prediction Error Formula

In this appendix, we will derive Eqs. (1) and (2). We wish to minimize

$$J = \sum_{i=1}^{N} [Z_i - (a_o + a_1 R_i)]^2 / \sigma_i^2$$

with respect to a_o and a_1. Differentiating, we obtain

$$\frac{\partial J}{\partial a_o} = 0 = \sum_i (a_o + a_1 R_i - Z_i) \ (1/\sigma_i^2)$$

$$\frac{\partial J}{\partial a_1} = 0 = \sum_i (a_o + a_1 R_i - Z_i) \ (R_i/\sigma_i^2)$$

We eliminate a_1 to obtain Eq. (1) for a_o

$$a_o = \frac{\sum \frac{Z_i}{\sigma_i^2} \ \sum \frac{R_i^2}{\sigma_i^2} - \sum \frac{R_i Z_i}{\sigma_i^2} \ \sum \frac{R_i}{\sigma_i^2}}{\sum \frac{1}{\sigma_i^2} \ \sum \frac{R_i^2}{\sigma_i^2} - \left(\sum \frac{R_i}{\sigma_i^2} \right)^2} \qquad (1)$$

The variance of a_o is the expected value of the square of the deviation of a_o from its expected value

$$\mathrm{Var}(a_o) = \left\langle (a_o - \langle a_o \rangle)^2 \right\rangle$$

From Eq. (1), we see that $\langle a_o \rangle = 0$ so

$$\mathrm{Var}(a_o) = \langle a_o^2 \rangle$$

In taking the variance of Eq. (1), we use the fact that

$$\langle Z_i \rangle = 0$$

$$\langle Z_i Z_j \rangle = \sigma_i^2 \, \delta_{ij}$$

which greatly reduces the number of terms to be saved. After some straightforward algebra, we obtain Eq. (2)

$$\mathrm{Var}(a_o) = \frac{\sum \frac{R_i^2}{\sigma_i^2}}{\sum \frac{1}{\sigma_i^2} \sum \frac{R_i^2}{\sigma_i^2} - \left(\sum \frac{R_i}{\sigma_i^2} \right)^2} \qquad (2)$$

APPENDIX 2: Derivation of Prediction Error Results

In this appendix we will derive Eqs. (5) and (6) from Eq. (3).

Case 0 Substituting $\sigma_R = \sigma$ into Eq. (3) gives

$$\mathrm{Var}(a_o) = \frac{V_c \sigma^2}{prf} \frac{\left(\frac{R_A^3 - R^3}{3}\right)}{(R_A - R)\left(\frac{R_A^3 - R^3}{3}\right) - \left(\frac{R_A^2 - R^2}{2}\right)^2}$$

which simplifies to

$$\mathrm{Var}(a_o) = \frac{4\, V_c\, \sigma^2}{prf} \frac{R_A^2 + R_A R + R^2}{(R_A - R)^3}$$

Letting $y \equiv R_A/R$ results in Eq. (5a). The limit $R \to R_A$ yields Eq. (6) directly.

Case 1 Substituting $\sigma_R = \sigma_\theta R$ into Eq. (3) gives

$$\mathrm{Var}(a_o) = \frac{V_c\, \sigma_\theta^2}{prf} \frac{R_A - R}{\left(\frac{1}{R} - \frac{1}{R_A}\right)(R_A - R) - \left(\ln \frac{R_A}{R}\right)^2}$$

which becomes Eq. (5b) on multiplication and substitution of y. It is more difficult to derive Eq. (6) in this case. Writing $y = 1 + \varepsilon$ and keeping terms to order ε^4 in the denominator of

Eq. (5b) , we obtain

$$f(y) = \frac{\varepsilon}{(1+\varepsilon) + (1-\varepsilon+\varepsilon^2-\varepsilon^3+\varepsilon^4)-2 - (\varepsilon - \frac{\varepsilon^2}{2} + \frac{\varepsilon^3}{3})}^2$$

$$f(y) = \frac{12}{\varepsilon^3} = \frac{12\ R^3}{(R_A-R)^3}$$

This yields Eq. (6).

Case 2 Substituting $\sigma_R = \sigma_A R^2/R_A$ into Eq. (3) gives

$$Var(a_o) = \frac{V_c\ \sigma_A^2}{prf \cdot R_A^2} \frac{\left(\frac{1}{R} - \frac{1}{R_A}\right)}{\frac{1}{3}\left(\frac{1}{R} - \frac{1}{R_A}\right)\left(\frac{1}{R^3} - \frac{1}{R_A^3}\right) - \frac{1}{4}\left(\frac{1}{R^2} - \frac{1}{R_A^2}\right)}^2$$

The calculation is simplified by the substitution $X \equiv 1/R$, $X_A = \frac{1}{R_A}$

$$Var(a_o) = \frac{V_c\ \sigma_A^2\ X_A^2}{prf} \frac{12}{(X-X_A)\ \left[4(X^2+XX_A+X_A^2)-3(X+X_A)^2\right]}$$

which simplifies to Eq.(5c). The limit of Eq. (6) is obtained directly.

Case 3 Substituting $\sigma_R = \sigma_A R^3/R_A^2$ into Eq. (3) gives

$$\mathrm{Var}(a_o) = \frac{V_c\,\sigma_A^2}{\mathrm{prf}\cdot R_A^4}\;\frac{\frac{1}{3}\left(\frac{1}{R^3}-\frac{1}{R_A^3}\right)}{\frac{1}{15}\left(\frac{1}{R^5}-\frac{1}{R_A^5}\right)\left(\frac{1}{R^3}-\frac{1}{R_A^3}\right)-\frac{1}{16}\left(\frac{1}{R^4}-\frac{1}{R_A^4}\right)^2}$$

Again we make the subtitution $X \equiv 1/R$ but the simplification is not as great as in Case 2. Removing some common factors of $(X-X_A)$, we obtain

$$\mathrm{Var}(a_o) = \frac{80\,V_c\sigma_A^2 X_A^4}{\mathrm{prf}\cdot(X-X_A)}\cdot$$

$$\cdot\;\frac{X^2+XX_A+X_A^2}{16(X^2+XX_A+X_A^2)(X^4+X^3X_A+X^2X_A^2+XX_A^3+X_A^4)-15\,(X^3+X^2X_A+XX_A^2+X_A^3)^2}$$

The terms in the denominator may be regrouped to yield Eq. (5d). Taking the limit $y\to 1+\varepsilon$ we must keep terms of order ε^3 in the denominator of $h(y)$. We obtain

$$h(y) = \frac{3}{\varepsilon\left[(4+6\varepsilon+4\varepsilon^2+\varepsilon^3)^2 - 16(1+3\varepsilon+3\varepsilon^2+\varepsilon^3)\right]}$$

$$h(y) = \frac{3}{20\varepsilon^3}$$

This yields Eq. (6).

APPENDIX 3: Nomogram Kit

In this Appendix, we give copies of 6 graphs which may be made into transparencies and overlayed appropriately to generate results similar to those given in Section IV. This Appendix gives instructions for making and using these nomograms.

Fig. A-1 is the base graph with two scales A-A and B-B giving various values of V_c. Figs. A-2 and A-5 contain graphs of prediction accuracy vs. range for 5 values of R_A. Scale A-A on these figures should be overlayed on scale A-A on Fig. A-1 with the appropriate value of $\sigma/\sqrt{prf/100}$ opposite the appropriate value of V_c. For a prf of 100, the values on scale A-A are just the measurement accuracies. For higher or lower values of prf, the effective measurement error will be lower or higher respectively. Using the appropriate combination of curves, the user can construct composite prediction error curves similar to Fig. 5 by eyeball.

Fig. A-6 contains graphs of divert capability vs. range for 4 values of τ. It also contains 4 horizontal lines for different maneuver limits and a vertical line for V_c. The appropriate line for the maneuver limit should be overlayed on scale B-B on Fig. A-1 and the vertical line should go through the appropriate value of V_c on scale B-B.

If 4 or 5 overlays are used simultaneously, the reader will undoubtedly suffer eye- or brain-strain. In this case it is

simpler to trace the appropriate curve or curves onto a fresh transparency or piece of tracing paper.

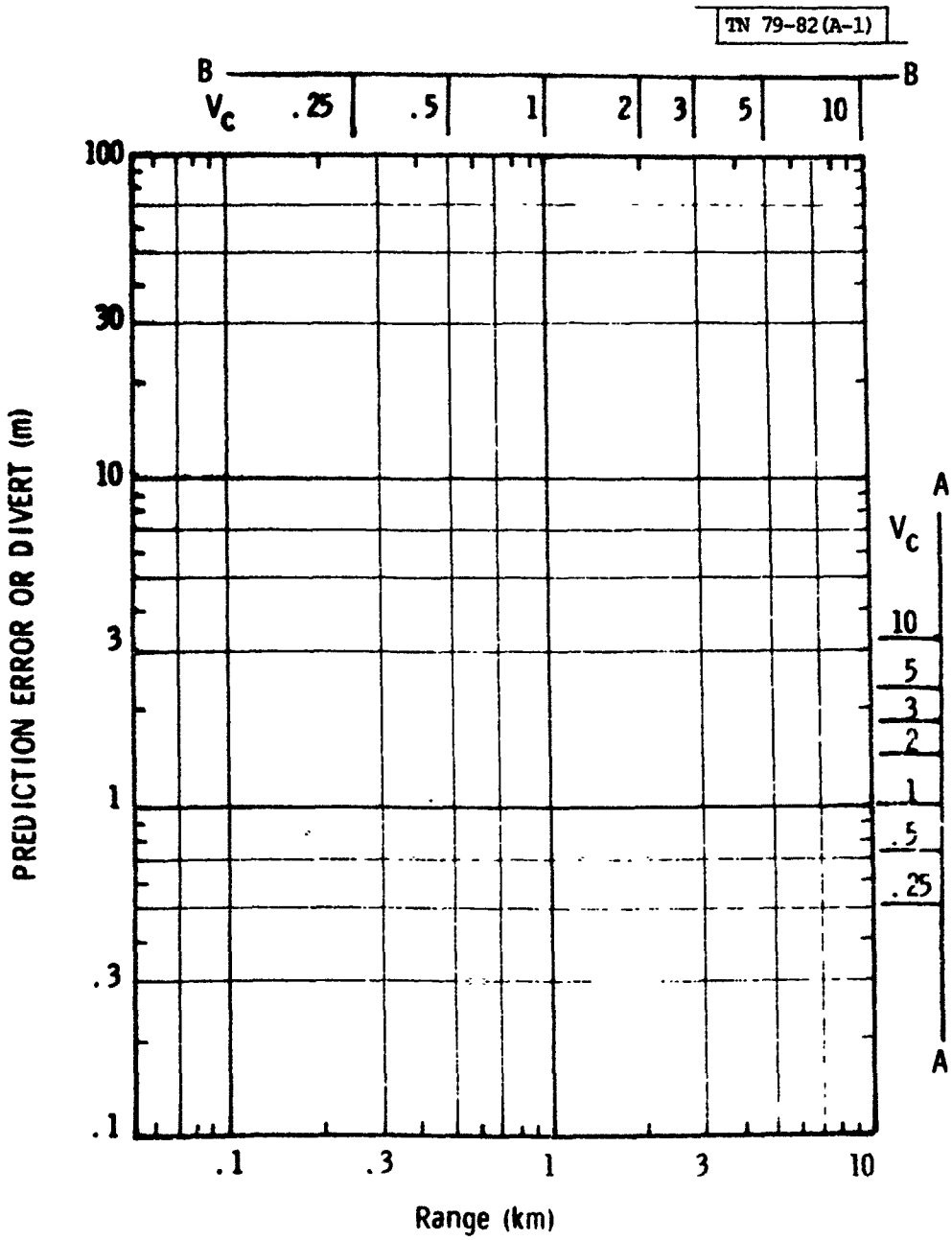

Fig. A-1. Nomogram base.

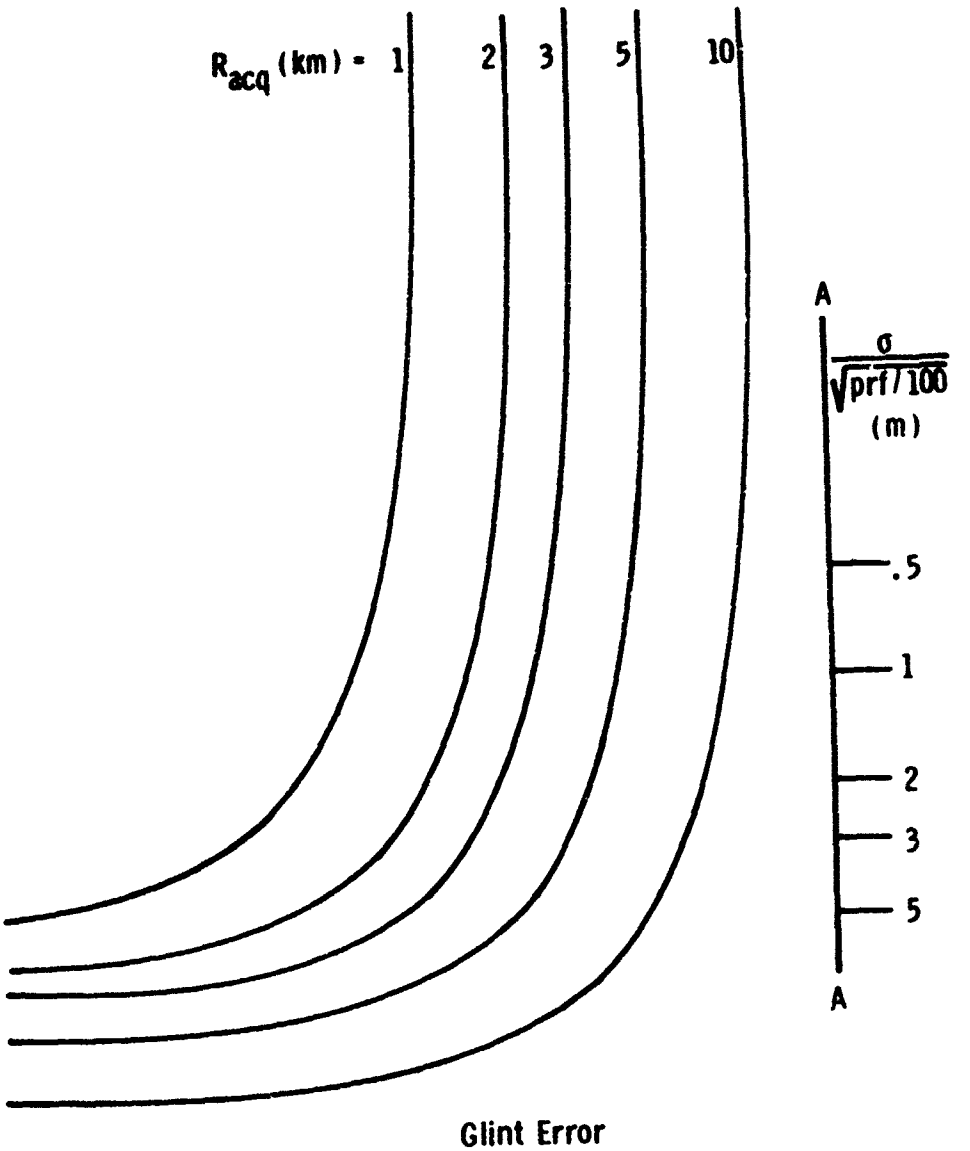

Fig. A-2. Glint overlay.

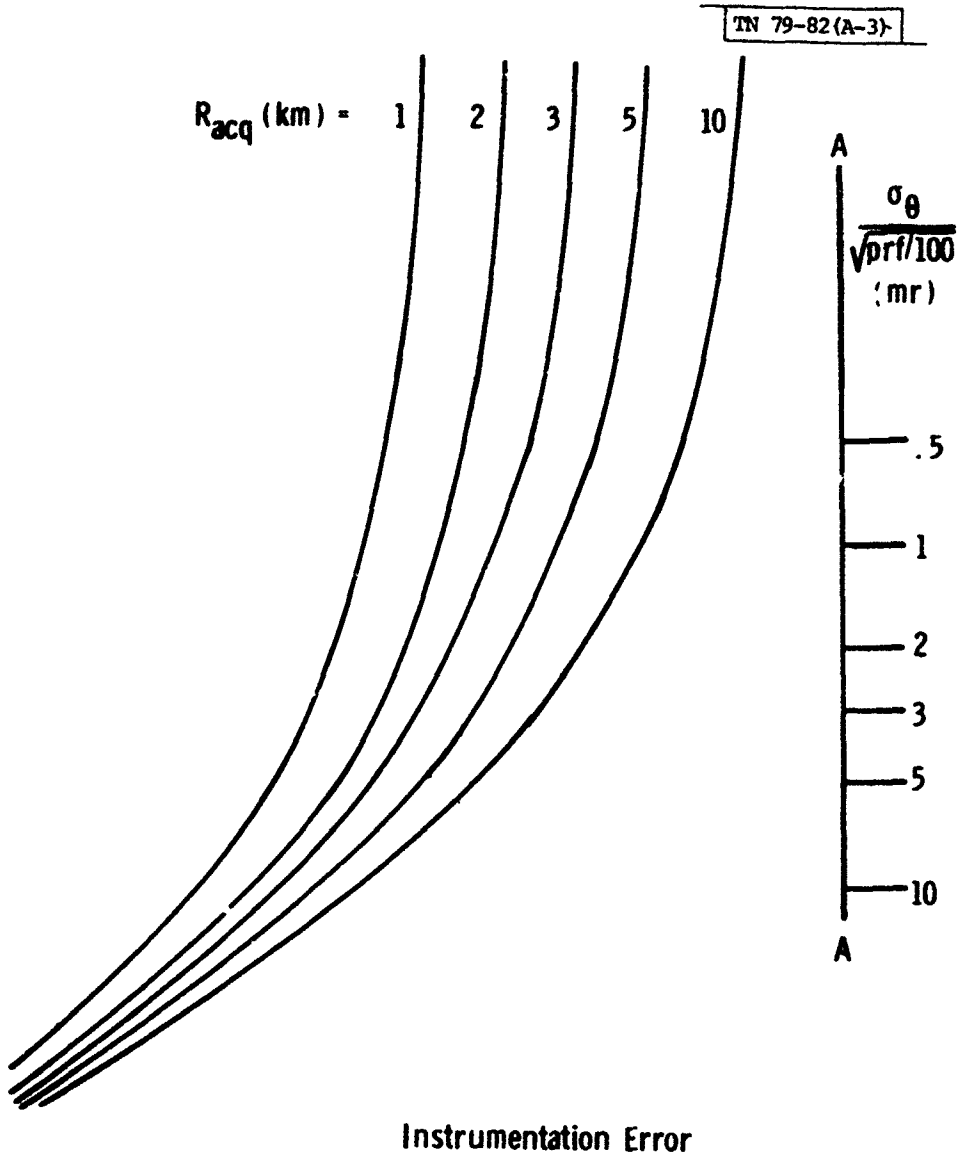

Instrumentation Error

Fig. A-3. Instrumentation overlay.

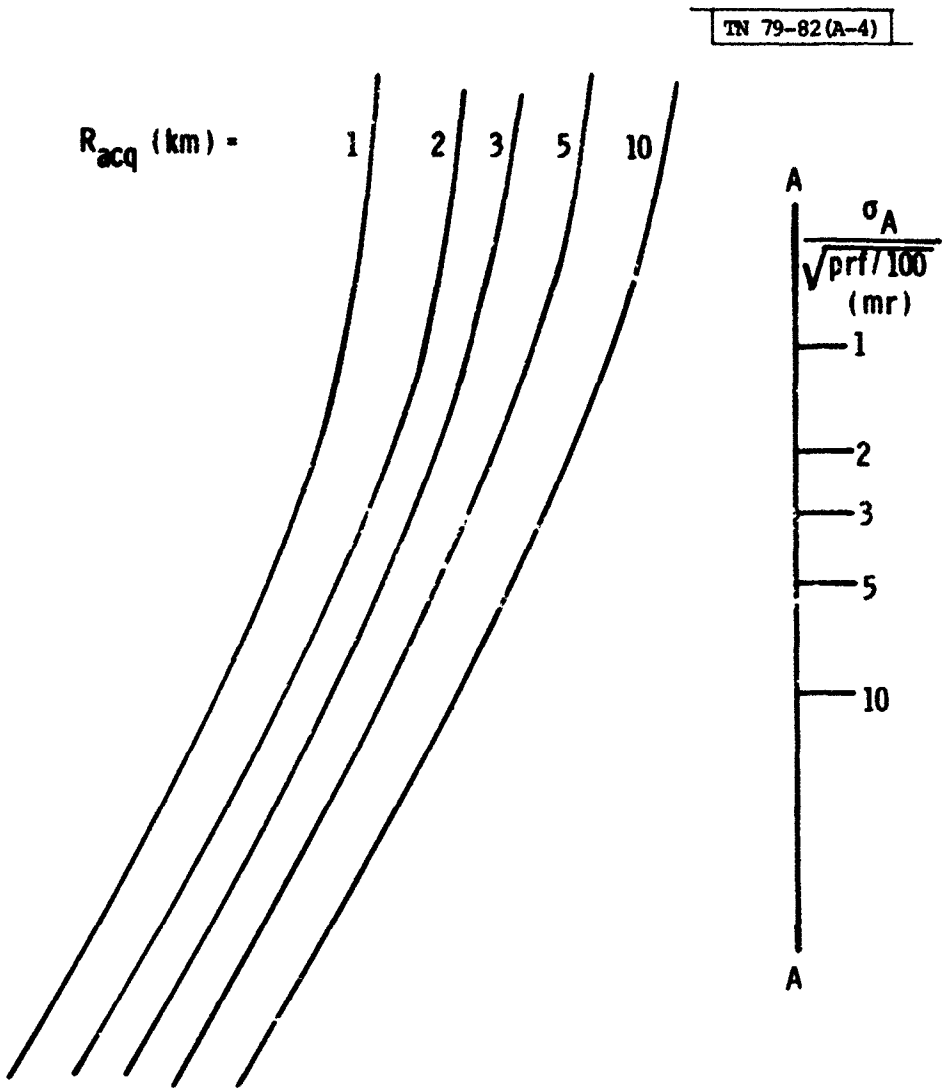

Thermal Error (Semi-active)

Fig. A-4. Thermal (semi-active) overlay.

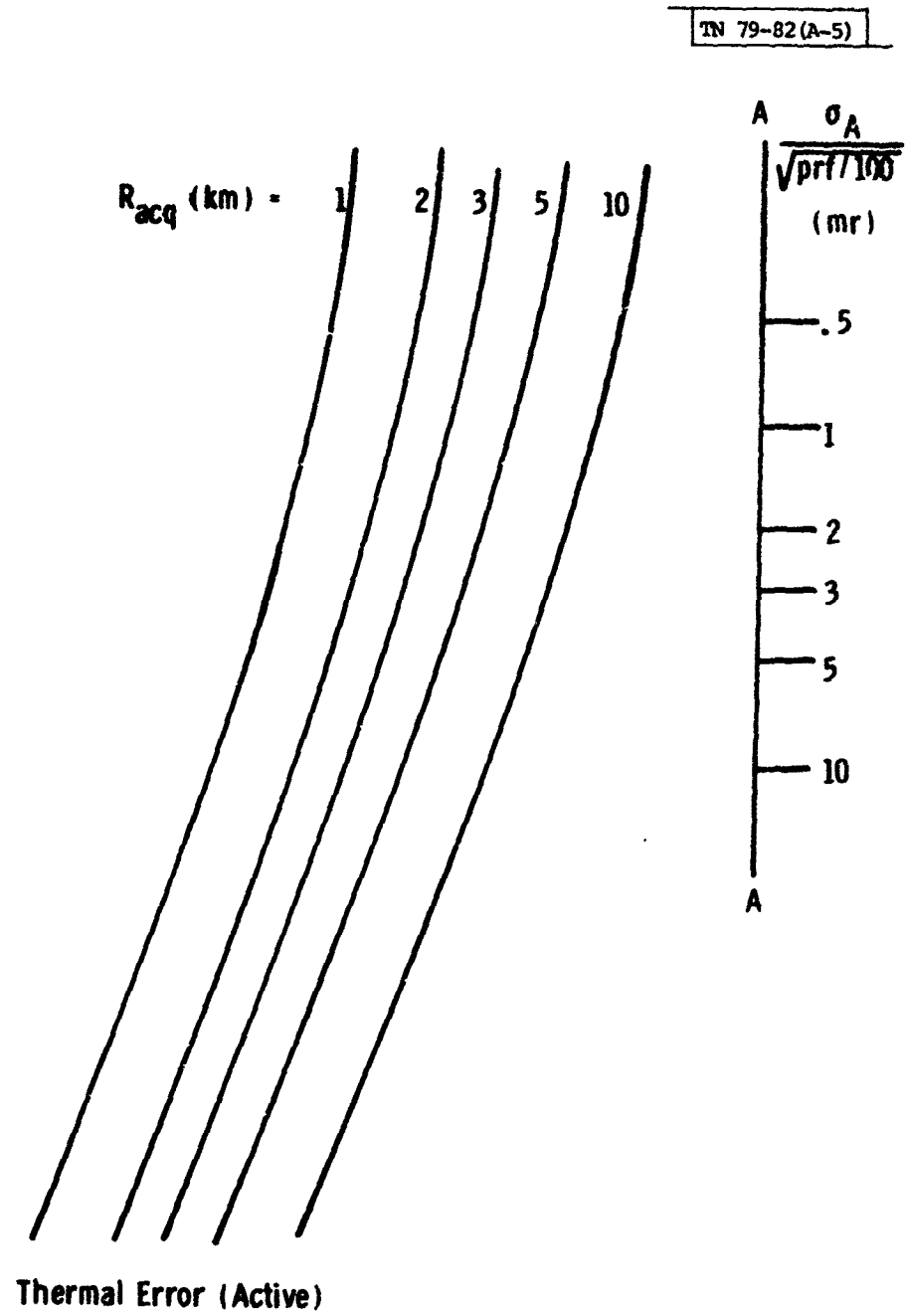

Fig. A-5. Thermal (active) overlay.

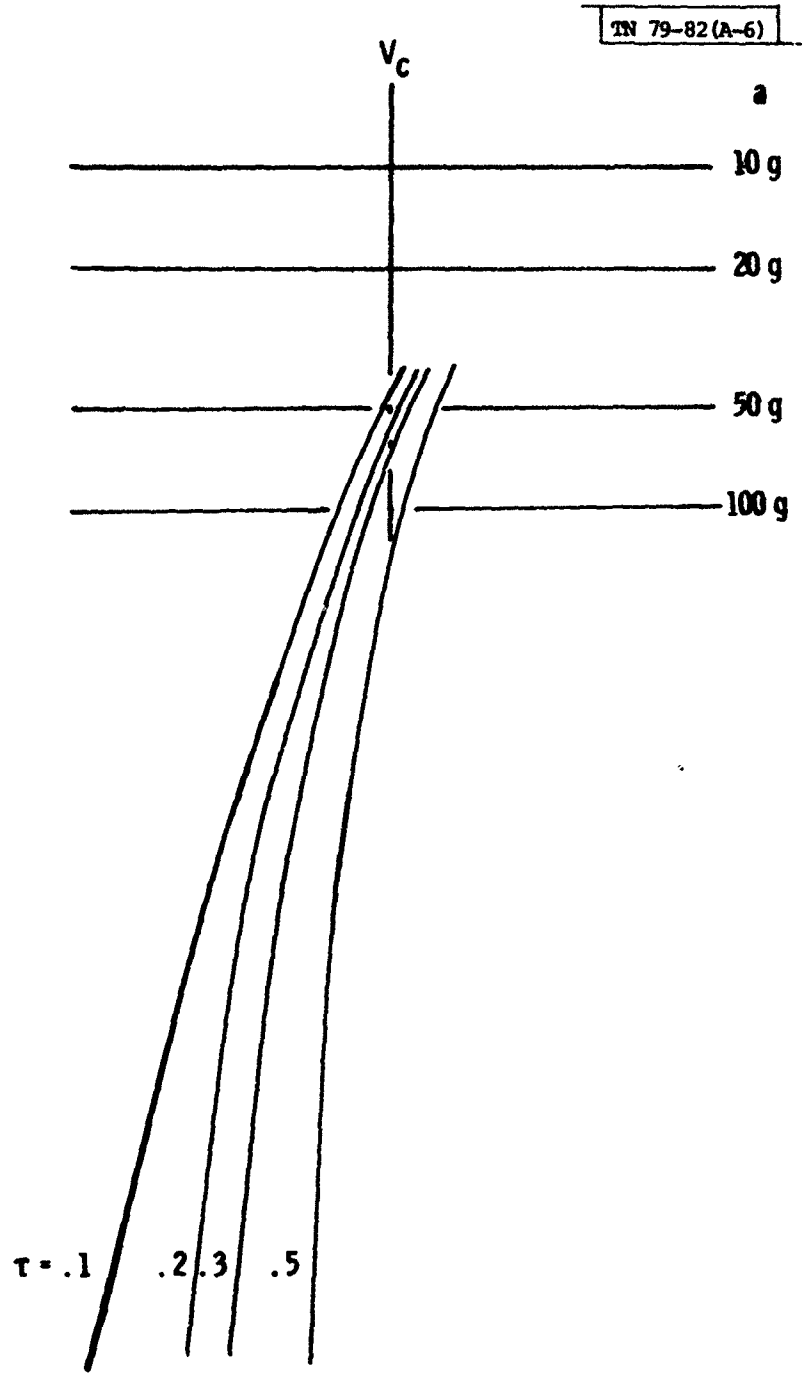

Fig. A-6. Interceptor overlay.

UNCLASSIFIED

SECURITY CLASSIFICATION OF THIS PAGE *(When Data Entered)*

(19) REPORT DOCUMENTATION PAGE		READ INSTRUCTIONS BEFORE COMPLETING FORM
1. REPORT NUMBER (13) ESD-TR-79-284	2. GOVT ACCESSION NO.	3. RECIPIENT'S CATALOG NUMBER
4. TITLE *(and Subtitle)* (6) A Simple Graphical Model for Analyzing Radar Homing Interceptor Engagements		5. TYPE OF REPORT & PERIOD COVERED (9) Technical Note 6. PERFORMING ORG. REPORT NUMBER Technical Note 1979-82
7. AUTHOR(s) (10) Stephen D. Weiner		8. CONTRACT OR GRANT NUMBER(s) (15) F19628-80-C-0002
9. PERFORMING ORGANIZATION NAME AND ADDRESS Lincoln Laboratory, M.I.T. P.O. Box 73 Lexington, MA 02173		10. PROGRAM ELEMENT, PROJECT, TASK AREA & WORK UNIT NUMBERS Program Element Nos. 63304A and 63308A
11. CONTROLLING OFFICE NAME AND ADDRESS Ballistic Missile Defense Program Office Department of the Army 5001 Eisenhower Avenue Alexandria, VA 22333		(11) 12. REPORT DATE 17 Dec 79 13. NUMBER OF PAGES 52
14. MONITORING AGENCY NAME & ADDRESS *(if different from Controlling Office)* Electronic Systems Division Hanscom AFB Bedford, MA 01731 (12) 50		15. SECURITY CLASS. *(of this report)* Unclassified 15a. DECLASSIFICATION DOWNGRADING SCHEDULE

16. DISTRIBUTION STATEMENT *(of this Report)*

Approved for public release; distribution unlimited.

(14) TN-1979-82

17. DISTRIBUTION STATEMENT *(of the abstract entered in Block 20, if different from Report)*

18. SUPPLEMENTARY NOTES

None

19. KEY WORDS *(Continue on reverse side if necessary and identify by block number)*

radar homing sensors
interception engagements
re-entry vehicles
sensor prediction accuracy
non-nuclear interception
prediction accuracy

20. ABSTRACT *(Continue on reverse side if necessary and identify by block number)*

In this note, a simplified model of radar homing interceptor engagements is described. This model permits analysis of the interaction among sensor parameters such as angular accuracy and acquisition range, nterceptor parameters such as maneuver limits and response time and system parameters such as closing velocity and handover accuracy. Simple expressions are obtained for the sensor prediction accuracy using various types of range-dependent measurement errors. These include glint, instrumentation error and thermal error for both active and semi-active sensors. A simple graphical technique is used to determine the feasibility of a homing engagement and to estimate the resulting miss-distance. A set of nomograms is included to permit full variation of the system and component parameters.

DD FORM 1 JAN 73 1473 EDITION OF 1 NOV 65 IS OBSOLETE

UNCLASSIFIED

SECURITY CLASSIFICATION OF THIS PAGE *(When Data Entered)*

207650